


 Cite this: *RSC Adv.*, 2024, 14, 15907

The impact of a TiO₂/r-GO composite material on the performance of electron transport electrodes of dye sensitized solar cells

 Hina Pervaiz,^a  [✉] Nadia Shahzad^{*a} and Qasim Jamil^b

In dye sensitized solar cells, the role of the electron transport layer is crucial because it makes it easier for photo-generated electrons to get from the dye to the external circuit. In DSSCs, the utilization of TiO₂ is likely to be given preference in the production of electron transport electrodes due to its notable characteristics such as its expansive surface area, porosity, and capacity to scatter light. Nevertheless, the presence of heterogeneity within the mesoporous structure increases the likelihood of TiO₂ aggregation, which subsequently diminishes the beneficial impact of TiO₂ on the performance of DSSCs. In this context, reduced graphene oxide (r-GO) is introduced as an additive into the TiO₂ network during the preparation of TiO₂/reduced graphene oxide (r-GO) composites. The integration of r-GO with TiO₂ has been recognized as a promising approach to enhance electron transport and electron lifespan, owing to remarkable qualities exhibited by r-GO. The present investigation involved the synthesis of a composite material including titanium dioxide/reduced graphene oxide (TiO₂/r-GO) through the utilization of the co-precipitation technique. Following this, the generated TiO₂/r-GO composite material and pure TiO₂ were deposited on FTO through electrophoretic deposition to obtain an electron transport electrode of a dye sensitized solar cell. It should be noted that when r-GO was combined with TiO₂, the performance of DSSCs improved notably compared to pure TiO₂. As a result, the findings of this work have significant implications for the advancement of the TiO₂/r-GO composite deposited through electrophoretic deposition. The power conversion efficiency reached 6.64% with the addition of r-GO in the metal oxide electron transport electrode. The obtained findings align with the outcomes of electrochemical impedance investigations in which the electrode constructed with TiO₂/r-GO exhibits reduced electron transport resistance (R_{ct}) at the anode/dye/electrolyte interface, as well as lower overall resistance (R_{total}) in comparison to TiO₂-based DSSCs. These advancements have the potential to be employed in commercial DSSC manufacturing.

 Received 1st February 2024
 Accepted 5th April 2024

DOI: 10.1039/d4ra00829d

rsc.li/rsc-advances

Introduction

Dye-sensitized solar cells (DSSCs), which represent third-generation solar cell technology, have had notable progress since the time of them being reported by Brian O'Regan and Michael Grätzel in 1991.¹ In comparison to silicon-based solar cells that were first developed in the 1940s, DSSCs have notable benefits including environmental sustainability, recyclability, and efficiency, particularly in the presence of artificial lighting conditions.²⁻⁴ Furthermore, the versatile and user-friendly nature of DSSCs presents researchers with prospects to investigate various materials and synthesis techniques with the objective of improving their total efficiency.⁵⁻⁷

The fundamental operational mechanism of DSSCs comes from the photovoltaic phenomenon, wherein photosensitizing dyes absorb energy from photons and further emit electrons that are transported through an electron transport electrode.⁸⁻¹⁰ To achieve optimal efficiency, it is imperative for electron transport electrode (photoanode) materials to fulfil the needs of possessing good dye absorption characteristics and possessing an acceptable band-gap energy. Therefore, the utilization of TiO₂ is likely to be given preference in the production of electron transport electrodes for DSSCs due to its notable characteristics such as its expansive surface area, porosity, and capacity to scatter light.¹¹⁻¹³ Nevertheless, the presence of heterogeneity within the mesoporous structure increases the likelihood of TiO₂ aggregation, which subsequently diminishes the beneficial impact of TiO₂ on the performance of DSSCs. Therefore, the use of TiO₂ in conjunction with diverse carbon-based materials, including carbon nanotubes, carbon nanorods, carbon quantum dots, and carbon nanofibers, to augment the efficiency of DSSCs has garnered significant interest from

^aU. S.-Pakistan Centre for Advanced Studies in Energy (USPCAS-E), National University of Sciences and Technology (NUST), H-12 Sector, 44000 Islamabad, Pakistan. E-mail: hpervaizphd19.ces@student.nust.edu.pk; nadia@uspcase.nust.edu.pk

^bFaculty of Chemistry and Chemical Technology, University of Ljubljana, Vecna Pot 113, SI-1000 Ljubljana, Slovenia



the global scientific community.^{14–16} The integration of r-GO with TiO₂ has been recognized as a promising approach to enhance electron transport and electron lifespan, owing to the remarkable qualities exhibited by r-GO.¹⁷ These properties include good thermal and electrical conductivity, a large specific surface area, and a membrane-like structure. Hence, TiO₂/r-GO composites can be made from their respective precursor components using co-precipitation synthesis. Furthermore, within the co-precipitation procedure, the incorporation of a reducing agent serves to produce r-GO sheets and improve the interconnection between TiO₂ NPs and r-GO sheets. Nevertheless, it is crucial to acknowledge that the co-precipitation approach may be subject to the direct involvement of the reducing agent in the synthesis of the composite material. Although prior studies have investigated diverse methodologies for material synthesis and corresponding reaction processes, there exists a scarcity of comprehensive research that has systematically examined the impacts of distinct reducing agents within identical experimental parameters. Hence, it is crucial to combine these impacts to facilitate the identification of the most suitable reducing agent for the required synthesis.

The present study involves the production of a TiO₂/r-GO composite material by the co-precipitation process, employing electrophoretic deposition for the fabrication of an electron transport electrode for dye sensitized solar cells. The produced electrodes were subjected to different analytical techniques for analysis.^{18,19} The role of r-GO in TiO₂ was investigated using the surface area enhancement technique and water contact angle to assess the hydrophilicity of the electrodes. Furthermore, photovoltaic and electrochemical testing was implemented to analyze the performance of electron transport electrodes of dye sensitized solar cells.

Experimental

Materials

Titanium tetraisopropoxide (C₁₂H₂₈O₄Ti, Sigma-Aldrich), acetic acid (CH₃COOH, Sigma-Aldrich), graphite powder (Merck), potassium permanganate (KMnO₄, Sigma-Aldrich), phosphoric acid (H₃PO₄, Sigma-Aldrich), sulfuric acid (H₂SO₄, Sigma-Aldrich), and hydrogen peroxide (H₂O₂, Sigma-Aldrich) were used for the synthesis of titanium dioxide, graphene oxide and the composite material. Furthermore, for electron transport electrode fabrication, fluorine-doped tin oxide (FTO)-coated glass was sourced from Sigma-Aldrich and N3 (*cis*-bis(isothiocyanato)bis(2,2'-bipyridyl-4,4'-dicarboxylato) ruthenium(II)) dye was acquired from Sigma-Aldrich for the sensitization of the photoanode. A Pt-based electrode was used as a counter electrode of DSSCs.

Iodine (I₂, Sigma-Aldrich), guanidine thiocyanate (GuSCN, Sigma-Aldrich), 1,2-dimethyl-3-propylimidazolium iodide (DMPII, Sigma-Aldrich), and 4-*tert*-butylpyridine (TBP, Sigma-Aldrich) were used for the preparation of the electrolyte that was used in the fabrication of devices. Last, lithium iodide (LiI, Sigma-Aldrich), lithium perchlorate (LiClO₄, Sigma-Aldrich) and acetonitrile (CH₃CN, Sigma-Aldrich) were used for electrochemical testing of the photoanode.

Synthesis of TiO₂/r-GO composite material

Graphene oxide (GO) was produced from graphite utilizing the Hummer's method, with a modification implemented in accordance with the procedure applied in previous work.²⁰ Using this, a suspension of GO was produced in deionized water at a concentration of 1 mg mL⁻¹ using ultrasonication. Titanium tetraisopropoxide (TTIP) was employed as a precursor in the processing of TiO₂. Initially, 5 mL of TTIP and 1 mL of acetic acid were dissolved together for 15 minutes at ambient temperature. Subsequently, a volume of 25 mL of deionized water was slowly introduced and agitated for a duration of 2 h to afford full hydrolysis of TiO₂. The GO suspension was subsequently added to the hydrolyzed TiO₂ solution while being subjected to magnetic stirring for a duration of 2 h at a temperature of 25 °C and a stirring speed of 600 rpm. To promote the reduction of GO and synthesis of titanium dioxide/reduced graphene oxide (TiO₂/r-GO) composite materials, hydrazine was injected into the solution.

Furthermore, the GO content was kept constant at 10% of the precursor mixture (TTIP and GO). The reducing agent, hydrazine, was introduced gradually in a consistent weight proportion of 4 mg per 1 mg of GO for a duration of 4 h, at 60 °C, and 600 rpm. The above process was repeated in the absence of GO and reducing agent to generate TiO₂ NPs, which were utilized as a reference sample. The resultant mixes were then centrifuged with deionized water at 4000 rpm to obtain suspensions. Subsequently, the suspensions were subjected to a thermal treatment at 450 °C for a duration of 5 h, resulting in the formation of TiO₂/r-GO composites as well as TiO₂ nanoparticles. Using an EPD process, electron transport electrodes of pure TiO₂ and TiO₂/r-GO composite material were then fabricated.²¹ In our previous research, the EPD fabrication process for electrodes is described.²² The overall process is shown in Fig. 1. For the deposition procedure, a homogenous suspension was prepared by stirring 0.2 g of TiO₂/r-GO composite powder in 50 mL of ethanol with 1 mL of distilled water. At room temperature, this mixture was agitated for 30 min. The electrodes (FTO glass) were immersed vertically in the prepared suspension and connected to a power supply to initiate the deposition process. The deposition process was conducted for 5 min at 20 V voltage to achieve a uniform deposition. Under the influence of an electric field, charged particles migrate towards an electrode surface during this process. The photoanode was rinsed with ethanol and dried at room temperature. Further, the electron transport electrode was placed in a furnace at 450 °C for 1 hour at a heating rate of 5 °C min⁻¹ before being cooled to ambient temperature. The entire procedure was repeated to create a pure TiO₂ electron transport electrode.

Characterization

X-ray diffraction (Bruker, Germany, D8 ADVANCE instrument fitted with a Cu K α radiation emitter. $\lambda = 1.5418 \text{ \AA}$) was performed for structural analysis at 25 kV operating power. Measurements were taken between 5° and 70° in 2 θ , advancing in step-scans of 0.02°. A multipoint Brunauer–Emmett–Teller (BET; Quantachrome NovaWin 2.0 instrument, Virginia) analyzer was used to



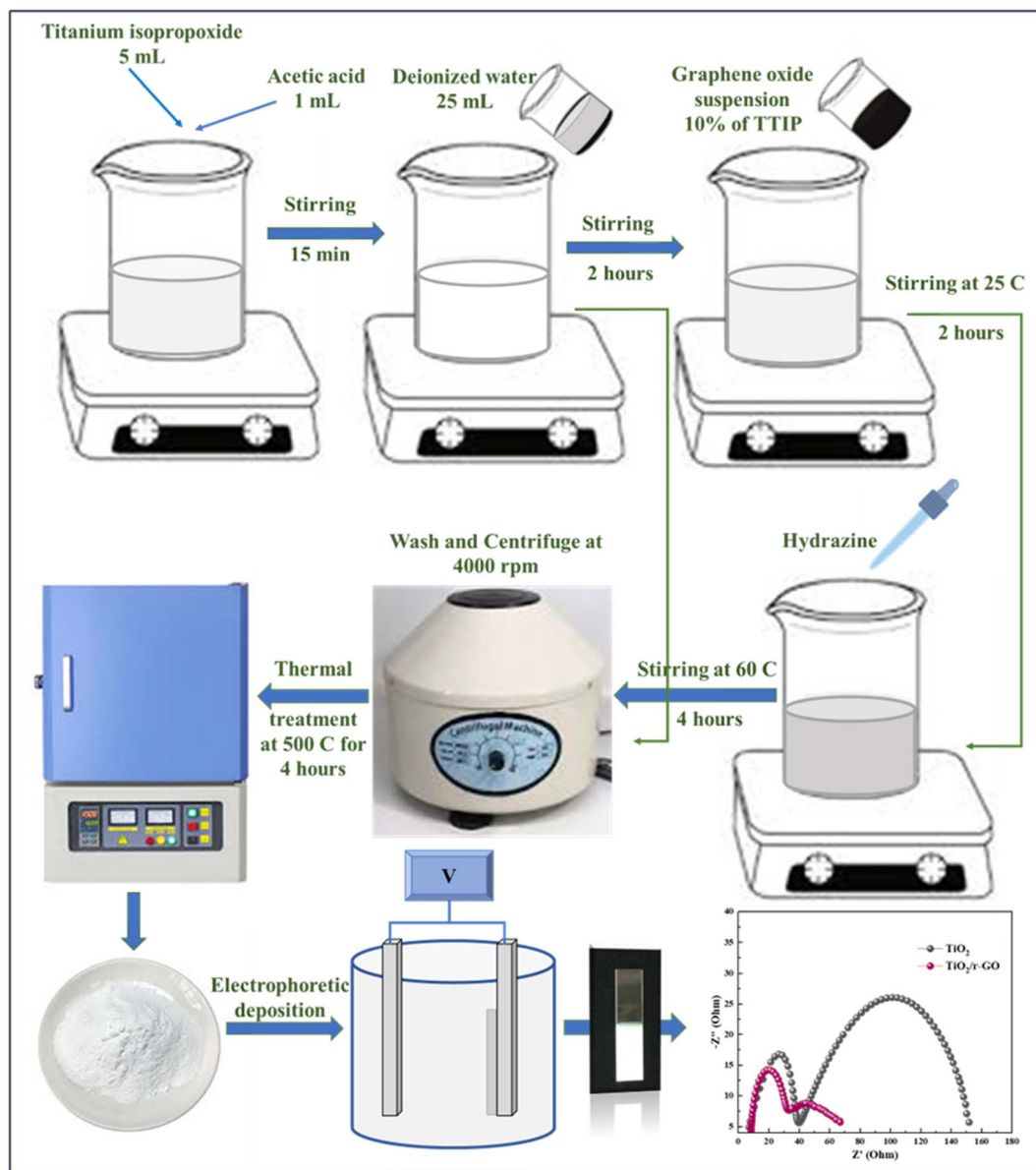


Fig. 1 Synthesis of $\text{TiO}_2/\text{r-GO}$ composite and electron transport electrode fabrication through electrophoretic deposition technique.

measure the surface area, pore volume, and pore size of the $\text{TiO}_2/\text{r-GO}$ composite material. This analysis was conducted on the sample using a volumetric apparatus, and nitrogen gas was used for the adsorption–desorption isotherm at a temperature of $-196\text{ }^\circ\text{C}$. Before the analysis, the sample was dried at a temperature of $150\text{ }^\circ\text{C}$ for 8 hours to eliminate moisture content.

The surface features of composite electrode film were examined using a TESCAN-MIRA3 SEM device. The images were captured at a field magnification ranging between $200\text{ }\mu\text{m}$ and 500 nm and employed an accelerating voltage varying from 15.0 to 10.0 kV . Further, the electron transport electrode was subjected to water contact angle measurement (VCA-OPTIMA) to assess the hydrophilicity of the TiO_2 nanoparticles and composite material.

A high-resolution X-ray photoelectron spectrometer (XPS) was employed to conduct elemental and chemical analyses of

the $\text{TiO}_2/\text{r-GO}$ composite. The full-scan, high-resolution spectra of different elements such as Ti 2p, C 1s, and O 1s were also recorded.

Electrochemical impedance spectroscopy (EIS) was conducted with dummy cells that had two identical electrodes and electrolyte solution in the frequency range of 10^{-1} to 10^5 Hz , utilizing an alternating current (AC) amplitude of 5 mV . The photovoltaic characterization of built DSSCs was conducted by measuring them using a solar simulator with an illumination intensity of 100 mW cm^{-2} .

Results and discussion

For structural analysis, XRD (Bruker, Germany) patterns of TiO_2 , $\text{TiO}_2/\text{r-GO}$ and r-GO were employed, as shown in Fig. 2. XRD profiles indicate that TiO_2 and r-GO are consistent with the



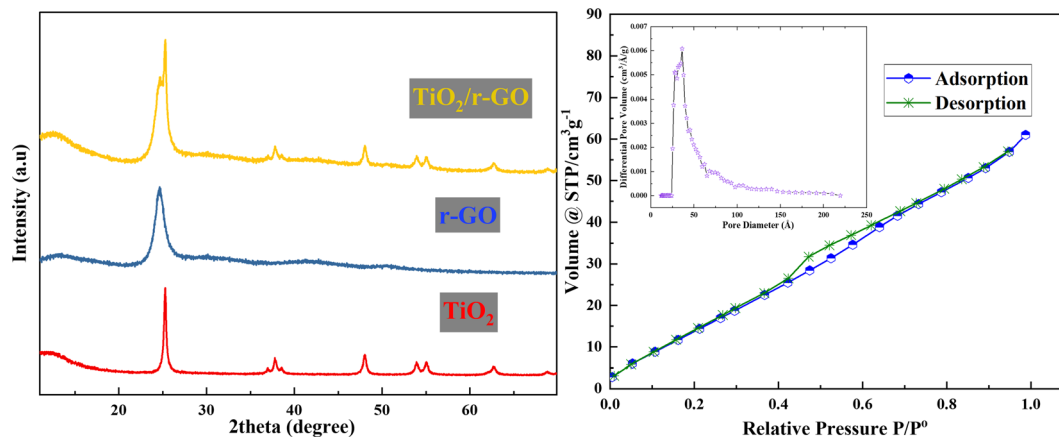


Fig. 2 XRD patterns of TiO_2 , r-GO, and $\text{TiO}_2/\text{r-GO}$ composite and adsorption–desorption curve of $\text{TiO}_2/\text{r-GO}$ composite.

literature. The profile of as-prepared TiO_2 is well matched with the standard tetragonal crystal system pattern of anatase of TiO_2 (73–1764). For r-GO, a distinct diffraction peak was observed at 24.6° , associated with the (002) crystal plane, denoting its highly organized structure. Further, the diffraction peaks of TiO_2 and r-GO are visible in the pattern of the composite material as seen in Fig. 2.

Using a BET surface area measurement tool, the surface characteristics of the $\text{TiO}_2/\text{r-GO}$ composite were evaluated. The composite powder was subjected to a pre-treatment process at a temperature of 150°C for a duration of 8 hours before the start of the analysis. A temperature of -196°C was used for the adsorption and desorption of nitrogen. Fig. 2 also shows the adsorption–desorption isotherm of $\text{TiO}_2/\text{r-GO}$ and pore size distribution curve. In accordance with the IUPAC classification, the $\text{TiO}_2/\text{r-GO}$ adsorption isotherm might be categorized as type II. The BET surface area was $54.989\text{ m}^2\text{ g}^{-1}$ for the $\text{TiO}_2/\text{r-GO}$ composite, which is greater than that of pure TiO_2 nanoparticles. Furthermore, this material is nano porous with an average pore radius of 1.795 nm and a pore volume of $0.088\text{ cm}^3\text{ g}^{-1}$, according to the Barrett–Joyner–Halenda (BJH) method.

Porous materials are more favorable for the electron transport electrodes of dye sensitized solar cells because high-surface-area materials allow greater amount of dye loading and improve electrolyte permeability.

In the current analysis, the addition of r-GO in the TiO_2 nanoparticles is accountable for enhanced dye loading and excellent electron transport. $\text{TiO}_2/\text{r-GO}$ with a desirable surface area is a promising composite material for superior dye loading. Further, it is capable of transferring charge through shorter paths. Wang *et al.* reported that a higher surface area of the electron transport electrode material is responsible for improved dye loading and excellent electron transport.²³ To probe the surface topography and structure of the composite film by TESCAN-MIRA3 scanning electron microscopy (SEM), $\text{TiO}_2/\text{r-GO}$ film was deposited on FTO/glass substrate. Fig. 3(a) and (b) show SEM images of the prepared $\text{TiO}_2/\text{r-GO}$ film at $200\text{ }\mu\text{m}$ and 500 nm , respectively. In Fig. 3(c), a water droplet on the $\text{TiO}_2/\text{r-GO}$ film to measure the contact angle can be seen. The wettability of a surface depends on two factors: its physical features like roughness and micro-/nanostructures and the inherent surface energy of the material itself.

The reason why the $\text{TiO}_2/\text{r-GO}$ composite performs better in converting light into energy compared to pure TiO_2 is linked to a reduction in the water contact angle, which was measured as 30.32° . A smaller contact angle means that dyes can cover the nanostructures more effectively, leading to enhanced photo-conversion efficiency.²⁴

The X-ray photoelectron spectroscopy (XPS) technique was utilized to conduct elemental and chemical analyses of the

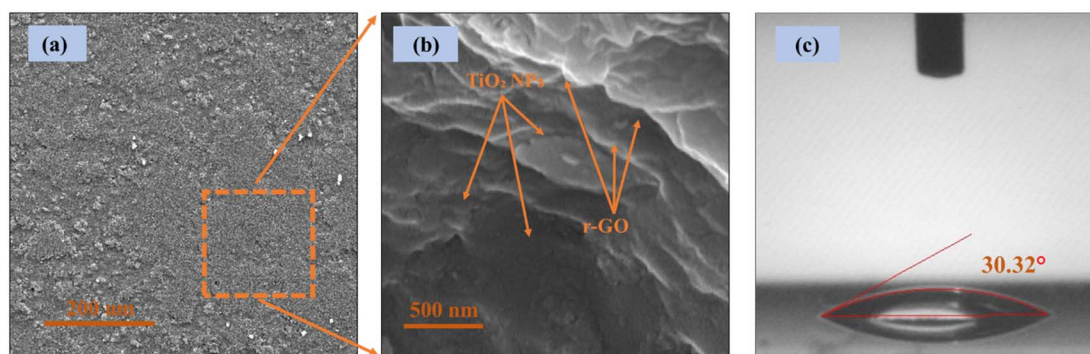


Fig. 3 (a and b) Scanning electron microscopy and (c) contact angle measurement of $\text{TiO}_2/\text{r-GO}$ composite film.



TiO₂/r-GO composite. The full-scan spectrum and high-resolution spectra of Ti 2p, C 1s, and O 1s are shown in Fig. 4.

In Fig. 4(a), a comprehensive analysis of TiO₂/r-GO reveals the presence of four prominent peaks at binding energies of approximately 284.5, 458.3, 466.5 and 533.0 eV. These peaks are attributed to C 1s, Ti 2p_{3/2}, Ti 2p_{1/2} and O 1s components, respectively. Other low-intensity peaks are also present in the full-scan spectrum. Fig. 4(b) illustrates the C 1s spectrum, deconvoluted into three peaks, attributed to different C bond types. The most noticeable peak is ascribed to the presence of C=C bonds at 283.7 eV, whereas the subsequent prominent peak is assigned to the presence sp³-hybridized C-C bonds at 285.0 eV, and the peak at 287.3 eV is associated with C-O-C bonds. The observed C 1s peaks reported in this paper are well aligned with the findings of Tien *et al.*²⁵ The signal associated with the O 1s peak (Fig. 4(c)) has been separated into three distinct peaks by deconvolution. The peak with the highest intensity at 532.1 eV is associated with C-O bonds. Moreover, peaks at 531.1 and 530.18 correspond to C-O-C and Ti-OH, respectively. The high-resolution spectrum of Ti 2p is shown in Fig. 4(d), which shows a doublet at 459.3 eV for Ti 2p_{3/2} and at 465.1 eV for Ti 2p_{1/2}. In the literature, the difference in the binding energies of Ti 2p_{3/2} and Ti 2p_{1/2} is about 5.8 eV, which is in agreement with the +4 oxidation state of Ti in the TiO₂

lattice.²⁶ A similar difference is observed in the current composition, which indicates the existence of Ti⁴⁺ in the prepared TiO₂/r-GO composite.

To analyze the electron transport resistance across different interfaces, we applied electrochemical impedance spectroscopy (EIS). This was done in a frequency range from 10⁵ Hz to 1 Hz, linked with an applied open circuit potential. In Fig. 5, prominent semicircles are evident for TiO₂/r-GO and TiO₂, indicating considerable electron transport resistances in these configurations. The data fitting procedure is represented by the Randles circuit model. Within the high-frequency spectrum, the visible semicircle can be attributed to the charge-transfer resistance (R_{counter}) occurring at the interface between the cathode and electrolyte. Additionally, the symbol R_s represents the sheet resistance, primarily attributed to the resistance of the FTO substrate utilized in the electrode production process. Table 1 presents the values of sheet resistance (R_s), interfacial charge-transfer resistance (R_{counter}), and various other factors. The resistance values obtained from the second semicircle, covering a frequency range of 1 to 100 Hz, indicate that the resistance at the anode/dye/electrolyte interface (R_{ct}) of TiO₂ (112 Ω) was greater than that of TiO₂/r-GO (34.31 Ω) composite electron transport electrode.

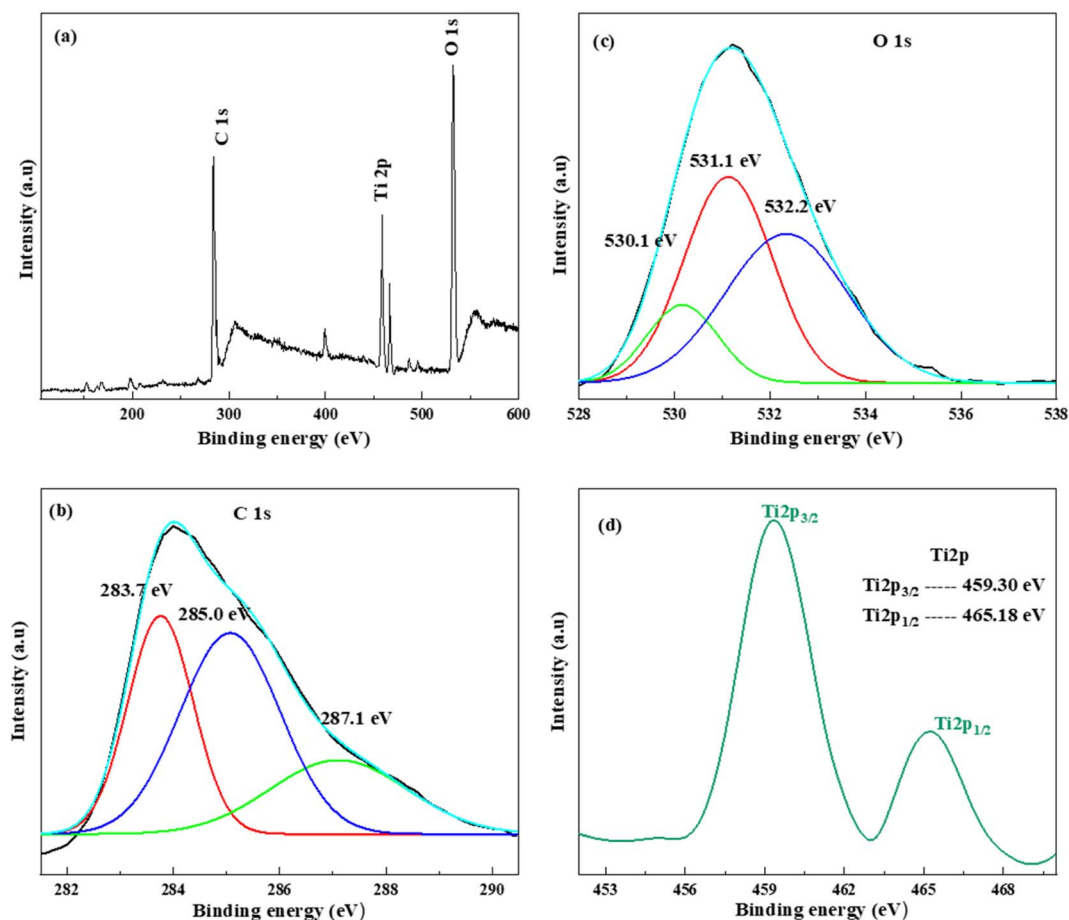


Fig. 4 (a) XPS full scan of TiO₂/r-GO, high-resolution spectra of (b) C 1s, (c) O 1s, and (d) Ti 2p.



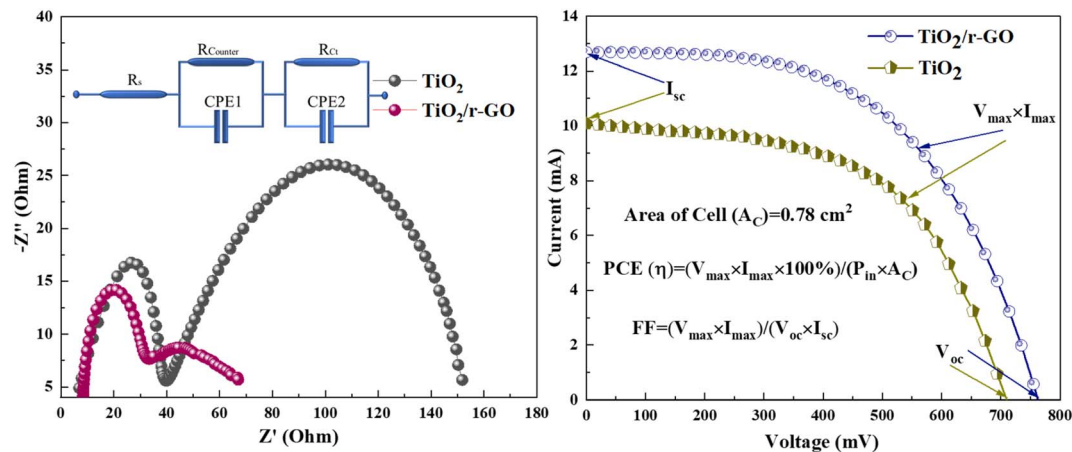


Fig. 5 Electrochemical impedance spectroscopy and current–voltage measurements of pure TiO_2 and $\text{TiO}_2/\text{r-GO}$ composite devices.

Table 1 EIS and I - V measurements of $\text{TiO}_2/\text{r-GO}$ - and TiO_2 -based dye sensitized solar cell devices

Electrode	R_s (Ω)	R_{counter} (Ω)	R_{ct} (Ω)	I_{sc} (mA)	V_{oc} (mV)	η (%)	FF (%)
$\text{TiO}_2/\text{r-GO}$	8.38	24.33	34.31	12.57	761	6.64	54.1
TiO_2	6.92	32.88	112	10.0	708	5.00	55.0

The total internal series resistance is equal to the sum of all these resistances (R_{total}). For DSSCs made of $\text{TiO}_2/\text{r-GO}$ and pure TiO_2 , the total internal resistance is 67.1 Ω and 151.6 Ω , respectively. The performance of the $\text{TiO}_2/\text{r-GO}$ electron transport electrode can be seen to be superior that of the TiO_2 one. In the literature, a similar electrochemical behaviour is reported, in which a cobalt sulfide nanostructure in comparison with Pt-based DSSCs is described, and cobalt sulfide has been proved to be very effective in catalyzing the redox electrolyte in DSSCs.²⁷

To understand complete performance of titanium dioxide/reduced graphene oxide ($\text{TiO}_2/\text{r-GO}$) and titanium dioxide (TiO_2) electron transport electrodes in DSSCs, photovoltaic (I - V) features were assessed using a power source while subjecting the devices to an illumination intensity of 100 mW cm^{-2} . Fig. 5 also shows the photovoltaic (I - V) characteristic curves of DSSCs using titanium dioxide/reduced graphene oxide ($\text{TiO}_2/\text{r-GO}$) and titanium dioxide (TiO_2) electron transport electrodes. The fill factor (FF) and power conversion efficiency (η) were computed from current voltage measurements, and the resulting values for all associated photovoltaic parameters are presented in Table 1. The findings indicate that a DSSC fabricated with a combination of TiO_2 and r-GO exhibits higher efficiency in comparison to a cell constructed with TiO_2 . Hence, the inclusion of r-GO can significantly increase the functioning of the device. In the literature, the performance of electron transport is dependent on the interaction between both materials. Thus, reduced graphene oxide (r-GO) possesses a planar structure with delocalized π -electrons, allowing them to form π - π stacking interactions with the titanium dioxide (TiO_2) nanoparticles. This stacking interaction can facilitate electron transfer between the r-GO

and TiO_2 nanoparticles. Here, in this work, the performance of the device showed the strong interaction between TiO_2 and r-GO in the nanocomposite.²⁸

The obtained findings align with the outcomes of the electrochemical impedance investigations. Specifically, the DSSC constructed with a $\text{TiO}_2/\text{r-GO}$ electrode exhibits reduced electron transport resistance (R_{ct}) at the anode/dye/electrolyte interface, as well as lower overall resistance (R_{total}) in comparison to TiO_2 -based DSSCs. Therefore, it can be observed that the performance of the $\text{TiO}_2/\text{r-GO}$ composite electrode surpasses that of the TiO_2 electrode. Hence, the higher efficiency of the $\text{TiO}_2/\text{r-GO}$ -based device as compared to others is mainly due to high surface area for dye absorption which is confirmed from BET surface area analysis and low contact angle.

Conclusion

Pure TiO_2 nanoparticles, $\text{TiO}_2/\text{r-GO}$ composite materials and their electron transport electrodes were successfully synthesized using the coprecipitation method and electrophoretic deposition technique. XRD patterns obtained from TiO_2 , r-GO, and the $\text{TiO}_2/\text{r-GO}$ composite provided evidence for the effective synthesis of these materials. The impact of reduced graphene oxide (r-GO) on the photovoltaic efficiency of DSSCs was demonstrated through higher BET surface area of 54.989 $\text{m}^2 \text{g}^{-1}$, reduced contact angle (30.32°) and the enhancement observed in the I_{sc} and PCE values of the DSSCs. Moreover, the resistance values derived from EIS spectra indicated the capacity of $\text{TiO}_2/\text{r-GO}$ composite materials to mitigate charge recombination and facilitate electron transport, hence boosting the performance of the DSSCs. Experimental findings indicate that the $\text{TiO}_2/\text{r-GO}$ composite material is a viable option for



constructing electron transport electrodes in DSSCs using the coprecipitation technique.

Conflicts of interest

The authors confirm that there are no evident conflicting financial interests or personal relationships that could have impacted the findings reported in this paper.

References

- 1 A. Hagfeldt, G. Boschloo, L. Sun, L. Kloo and H. Pettersson, *Dye-Sensitized Sol. Cells*, 2010, 6595–6663.
- 2 M. Ye, X. Wen, M. Wang, J. Iocozzia, N. Zhang, C. Lin and Z. Lin, Recent advances in dye-sensitized solar cells: From photoanodes, sensitizers and electrolytes to counter electrodes, *Mater. Today*, 2015, **18**, 155–162, DOI: [10.1016/j.mattod.2014.09.001](https://doi.org/10.1016/j.mattod.2014.09.001).
- 3 N. Mariotti, M. Bonomo, L. Fagioliari, N. Barbero, C. Gerbaldi, F. Bella and C. Barolo, Recent advances in eco-friendly and cost-effective materials towards sustainable dye-sensitized solar cells, *Green Chem.*, 2020, **22**, 7168–7218, DOI: [10.1039/d0gc01148g](https://doi.org/10.1039/d0gc01148g).
- 4 C. Longo and M. A. De Paoli, Dye-Sensitized Solar Cells: A Successful Combination of Materials, *J. Braz. Chem. Soc.*, 2003, **14**, 889–901, DOI: [10.1590/S0103-50532003000600005](https://doi.org/10.1590/S0103-50532003000600005).
- 5 K. Sharma, V. Sharma and S. S. Sharma, Dye-Sensitized Solar Cells: Fundamentals and Current Status, *Nanoscale Res. Lett.*, 2018, **13**, 381, DOI: [10.1186/s11671-018-2760-6](https://doi.org/10.1186/s11671-018-2760-6).
- 6 N. Shahzad, Lutfullah, T. Perveen, D. Pugliese, S. Haq, N. Fatima, S. M. Salman, A. Tagliaferro and M. I. Shahzad, Counter electrode materials based on carbon nanotubes for dye-sensitized solar cells, *Renewable Sustainable Energy Rev.*, 2022, **159**, 112196, DOI: [10.1016/j.rser.2022.112196](https://doi.org/10.1016/j.rser.2022.112196).
- 7 L. Song, P. Chen, Z. Li, P. Du, Y. Yang, N. Li and J. Xiong, Flexible carbon nanotubes/TiO₂/C nanofibrous film as counter electrode of flexible quasi-solid dye-sensitized solar cells, *Thin Solid Films*, 2020, **711**, 138307, DOI: [10.1016/j.tsf.2020.138307](https://doi.org/10.1016/j.tsf.2020.138307).
- 8 J. E. Ikpesu, S. E. Iyuke, M. Daramola and A. O. Okewale, Synthesis of improved dye-sensitized solar cell for renewable energy power generation, *Sol. Energy*, 2020, **206**, 918–934, DOI: [10.1016/j.solener.2020.05.002](https://doi.org/10.1016/j.solener.2020.05.002).
- 9 S. Rahman, A. Haleem, M. Siddiq, M. K. Hussain, S. Qamar, S. Hameed and M. Waris, Research on dye sensitized solar cells: recent advancement toward the various constituents of dye sensitized solar cells for efficiency enhancement and future prospects, *RSC Adv.*, 2023, **13**, 19508–19529, DOI: [10.1039/d3ra00903c](https://doi.org/10.1039/d3ra00903c).
- 10 S. Rahman, A. Haleem, M. Siddiq, M. K. Hussain, S. Qamar, S. Hameed and M. Waris, Research on dye sensitized solar cells: recent advancement toward the various constituents of dye sensitized solar cells for efficiency enhancement and future prospects, *RSC Adv.*, 2023, **13**, 19508–19529, DOI: [10.1039/d3ra00903c](https://doi.org/10.1039/d3ra00903c).
- 11 A. Omar, M. S. Ali and N. Abd Rahim, Electron transport properties analysis of titanium dioxide dye-sensitized solar cells (TiO₂-DSSCs) based natural dyes using electrochemical impedance spectroscopy concept: A review, *Sol. Energy*, 2020, **207**, 1088–1121, DOI: [10.1016/j.solener.2020.07.028](https://doi.org/10.1016/j.solener.2020.07.028).
- 12 A. T. Raghavender, A. P. Samantilleke, P. Sa, B. G. Almeida, M. I. Vasilevskiy and N. H. Hong, Simple way to make Anatase TiO₂ films on FTO glass for promising solar cells, *Mater. Lett.*, 2012, **69**, 59–62, DOI: [10.1016/j.matlet.2011.11.067](https://doi.org/10.1016/j.matlet.2011.11.067).
- 13 W. Buraso, V. Lachom, P. Siriya and P. Laokul, Synthesis of TiO₂ nanoparticles via a simple precipitation method and photocatalytic performance, *Mater. Res. Express*, 2018, **5**(11), 115003, DOI: [10.1088/2053-1591/aadbfo](https://doi.org/10.1088/2053-1591/aadbfo).
- 14 S. Mahalingam, A. Manap, R. Rabeya, K. S. Lau, C. H. Chia, H. Abdullah, N. Amin and P. Chelvanathan, Electron transport of chemically treated graphene quantum dots-based dye-sensitized solar cells, *Electrochim. Acta*, 2023, **439**, 141667, DOI: [10.1016/j.electacta.2022.141667](https://doi.org/10.1016/j.electacta.2022.141667).
- 15 M. Wu, X. Lin, T. Wang, J. Qiu and T. Ma, Low-cost dye-sensitized solar cell based on nine kinds of carbon counter electrodes, *Energy Environ. Sci.*, 2011, **4**, 2308–2315, DOI: [10.1039/c1ee01059j](https://doi.org/10.1039/c1ee01059j).
- 16 H. Siddiqui, U. Ali, I. A. Sahito, S. A. Malik, K. C. Sun and N. Mengal, Comprehensive review of carbon materials as counter electrodes in dye-sensitized solar cells: Efficiency assessment and deposition methods, *Mater. Sci. Semicond. Process.*, 2024, **172**, 108074, DOI: [10.1016/j.mssp.2023.108074](https://doi.org/10.1016/j.mssp.2023.108074).
- 17 N. Wang, L. Cheng, Y. Liao and Q. Xiang, Effect of Functional Group Modifications on the Photocatalytic Performance of g-C₃N₄, *Small*, 2023, **19**, 2300109, DOI: [10.1002/sml.202300109](https://doi.org/10.1002/sml.202300109).
- 18 S. Ghannadi, H. Abdizadeh, A. Rakhsha and M. R. Golobostanfard, Sol-electrophoretic deposition of TiO₂ nanoparticle/nanorod array for photoanode of dye-sensitized solar cell, *Mater. Chem. Phys.*, 2021, **258**, 123893, DOI: [10.1016/j.matchemphys.2020.123893](https://doi.org/10.1016/j.matchemphys.2020.123893).
- 19 S. Shakir, H. M. Abd-ur-Rehman, R. Zahid, M. Iwamoto and V. Periasamy, Multistep electrophoretic deposition of TiO₂ film and its surface modification for dye sensitized solar cells, *J. Alloys Compd.*, 2020, **837**, 155579, DOI: [10.1016/j.jallcom.2020.155579](https://doi.org/10.1016/j.jallcom.2020.155579).
- 20 L. Van Cuong, D. Lam Tuan Cuong, L. Tran Trung Nghia, L. Khac Hung, N. Thai Hoang, L. Tan Nhiem, P. Trong Liem Chau, M. Thanh Phong and N. Huu Hieu, Effect of reducing agents on co-precipitation synthesis of titanium dioxide/reduced graphene oxide composite materials for upgrading the performance of dye-sensitized solar cells, *Chem. Eng. Sci.*, 2022, **264**, 118145, DOI: [10.1016/j.ces.2022.118145](https://doi.org/10.1016/j.ces.2022.118145).
- 21 S. Cabanas-Polo and A. R. Boccaccini, Electrophoretic deposition of nanoscale TiO₂: Technology and applications, *J. Eur. Ceram. Soc.*, 2016, **36**, 265–283, DOI: [10.1016/j.jeurceramsoc.2015.05.030](https://doi.org/10.1016/j.jeurceramsoc.2015.05.030).
- 22 H. Pervaiz, Z. S. Khan, N. Shahzad, N. Ahmed and Q. Jamil, Synthesis and characterization of CuInS₂ nanostructures and their role in solar cell applications, *Mater. Chem. Phys.*,



- 2022, **290**, 126602, DOI: [10.1016/j.matchemphys.2022.126602](https://doi.org/10.1016/j.matchemphys.2022.126602).
- 23 Z. S. Wang, H. Kawauchi, T. Kashima and H. Arakawa, Significant influence of TiO₂ photoelectrode morphology on the energy conversion efficiency of N719 dye-sensitized solar cell, *Coord. Chem. Rev.*, 2004, **248**, 1381–1389, DOI: [10.1016/j.ccr.2004.03.006](https://doi.org/10.1016/j.ccr.2004.03.006).
- 24 S. A. Mahadik, R. G. Sonkawade, F. Pedraza, L. B. Phadatare, A. K. Bhagate and M. R. Waikar, Enhancing photoelectrochemical performance through surface engineering of CdSe and Al-doped CdSe nanoparticles on ZnO/FTO photoanodes, *Int. J. Hydrogen Energy*, 2023, **51**, 676–689, DOI: [10.1016/j.ijhydene.2023.08.299](https://doi.org/10.1016/j.ijhydene.2023.08.299).
- 25 H. W. Tien, Y. L. Huang, S. Y. Yang, J. Y. Wang and C. C. M. Ma, The production of graphene nanosheets decorated with silver nanoparticles for use in transparent, conductive films, *Carbon N. Y.*, 2011, **49**, 1550–1560, DOI: [10.1016/j.carbon.2010.12.022](https://doi.org/10.1016/j.carbon.2010.12.022).
- 26 N. Sun, J. Ma, C. Wang, J. Xue, L. Qiang and J. Tang, A facile and efficient method to directly synthesize TiO₂/rGO with enhanced photocatalytic performance, *Superlattices Microstruct.*, 2018, **121**, 1–8, DOI: [10.1016/j.spmi.2018.07.017](https://doi.org/10.1016/j.spmi.2018.07.017).
- 27 K. Ashok Kumar, A. Pandurangan, S. Arumugam and M. Sathiskumar, Effect of Bi-functional Hierarchical Flower-like CoS Nanostructure on its Interfacial Charge Transport Kinetics, Magnetic and Electrochemical Behaviors for Supercapacitor and DSSC Applications, *Sci. Rep.*, 2019, **9**, 1–17, DOI: [10.1038/s41598-018-37463-0](https://doi.org/10.1038/s41598-018-37463-0).
- 28 N. T. Padmanabhan, N. Thomas, J. Louis, D. T. Mathew, P. Ganguly, H. John and S. C. Pillai, Graphene coupled TiO₂ photocatalysts for environmental applications: A review, *Chemosphere*, 2021, **271**, 12950, DOI: [10.1016/j.chemosphere.2020.129506](https://doi.org/10.1016/j.chemosphere.2020.129506).

